ACS APPLIED MATERIALS & INTERFACES

Research Article

www.acsami.org

High Aspect-Ratio Iridium-Coated Nanopillars for Highly Reproducible Surface-Enhanced Raman Scattering (SERS)

Guoguo Kang,*[,†,‡] Antti Matikainen,[‡] Petri Stenberg,[‡] Elina Färm,[§] Peng Li,[†] Mikko Ritala,[§] Pasi Vahimaa,[‡] Seppo Honkanen,[‡] and Xiaodi Tan[†]

[†]School of Optoelectronics, Beijing Institute of Technology, Beijing 100081, China

[‡]Institute of Photonics, University of Eastern Finland (Joensuu Campus), P.O. Box 111, FI-80101Joensuu, Finland

[§]Laboratory of Inorganic Chemistry, Department of Chemistry, University of Helsinki, P.O. Box 55, FI-00014, Helsinki, Finland

Supporting Information

ABSTRACT: A variety of different gold and silver nanostructures have been proposed over the years as high sensitivity surface-enhanced Raman scattering (SERS) sensors. However, efficient use of SERS has been hindered by the difficulty of realizing SERS substrates that provide reproducible SERS response over the whole active area. Here, we show that atomic layer deposition (ALD) grown iridium can be used to produce highly reliable SERS substrates. The substrates are based on a periodic array of high aspect-ratio iridium coated nanopillars that feature efficient and symmetrically distributed hot spots within the interpillar gaps (gap width < 10 nm). We show that the enhancement with the iridium based nanostructures is of significant magnitude and it equals the enhancement of silver based reference substrates. Most notably, we demonstrate that the ordered and well-defined plasmonic nanopillars offer a measurement-to-measurement variability of 5%, which paves the way for truly quantitative SERS measurements.

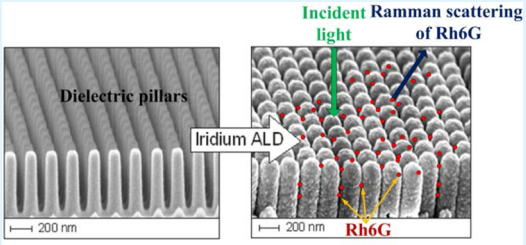

KEYWORDS: *plasmonic nanopillars, iridium, surface-enhanced Raman scattering (SERS), atomic layer deposition (ALD), localized surface plasmons (LSPs), nanogap, biosensor*

INTRODUCTION

Surface plasmons, the collective electron oscillations at metal−dielectric interfaces, have been widely utilized to enhance the light-matter interaction[1−3]for applications in chemical and biological sensing. Two types of surface plasmons (SPs), that is, surface plasmon polaritons (SPPs)[4,5] propagating on optically thin metal film and localized surface plasmons (LSPs)[6−10] that exhibit large localized electromagnetic fields within nanogaps, are used in surface-based sensing. The "hot spots", referring to the extremely intense and highly confined electromagnetic fields induced by the LSPs, are capable of enhancing many optical processes, such as absorption and scattering. These hot spots, which provide a large increase in absorption of the incident laser light and in the scattering cross-section of the adsorbed molecules, are crucial for surface-enhanced Raman scattering (SERS).

Because of the specific identification of chemical bonds, SERS is considered as one of the most promising approaches for highly accurate sensing, even down to a single-molecule level.[11,12] Chasing for higher sensitivity, great efforts have been taken to obtain enhancement values as large as possible.[13−15] However, besides the large enhancement, the detection of low levels of species is closely related to the probability of a molecule interacting with those hot-spot areas that provide large enough enhancement for sensing. In developing SERS substrates, the focus has primarily been on achieving enhancement values that may enable even the single-molecule detection. However, the variability between different points on the substrate is typically quite large, which leads to the average enhancement being significantly reduced in comparison with the maximum enhancement. Therefore, in the case of practical and quantitative measurements, having the molecules at nm-sized hot-spot areas is one of the key challenges.

Gold or silver are habitually used SERS materials because of their suitable plasmonic properties in the visible region. However, there are some limitations when using these materials. Silver for example, oxidizes easily, which leads to quick reduction in the SERS enhancement.[16] Gold, on the other hand, is resistant to atmospheric corrosion but inherently provides significantly lower signal enhancement than silver. Also some more exotic metals (especially from the platinum group), such as rhodium and ruthenium[17] and palladium and platinum[18] have been reported to possess some degree of SERS activity. Another interesting metal from this same group is iridium, which has also been recently demonstrated to possess SERS activity by using chains of nanoparticle assemblies.[19]

In this Research Article, we take the use of iridium in SERS to a next level and apply electron beam patterning and atomic

Received: March 12, 2015
Accepted: May 11, 2015
Published: May 11, 2015

DOI: 10.1021/acsami.5b02206
ACS Appl. Mater. Interfaces 2015, 7, 11452−11459

layer deposition (ALD) to fabricate symmetric arrays of iridium-coated high-aspect ratio nanopillars. ALD is a unique thin film deposition method based on saturative surface reactions of alternately supplied precursor vapors.[20,21] Because of the saturation of each reaction step, the film growth is self-limiting, thereby enabling conformal growth with atomic level control of film thickness. The goal of the highly controlled deposition is to overcome the notorious repeatability issues of SERS substrates. We optimize the geometry of the pillar structures through rigorous simulations in such a way that the nanopillar structures support highly enhanced fields within the interpillar gaps. We evaluate the performance of the iridium coated SERS substrates in terms of signal enhancement and measurement-to-measurement repeatability. We show that the enhancement depends on the interpillar gap width as well as the roughness of the film. Finally, we compare the enhancement and measurement repeatability of the iridium structures against different reference silver SERS substrates.

RESULTS AND DISCUSSION

Design and Theoretical Modeling. An ideal SERS substrate should provide high signal enhancement with high repeatability and thus, the signal enhancing hot spots should be efficient and also densely and uniformly distributed. A schematic representation of the proposed SERS substrate, which aims to achieve both of these goals, is shown in Scheme 1. It consists of a two-dimensional array of dielectric nanopillars, which are conformally coated with iridium. The purpose of this kind of a symmetric, high aspect-ratio grating structure is to provide both a large SERS active surface area and a uniform distribution of hot spots within the interpillar gaps. However, to effectively confine light within the interpillar gaps, the parameters (d = period, w_p= pillar width, h_p = pillar height, h_c = coating thickness, and g = interpillar gap width) of the structure have to be properly designed.

Scheme 1. Schematic Illustration of the Proposed SERS Structure[a]

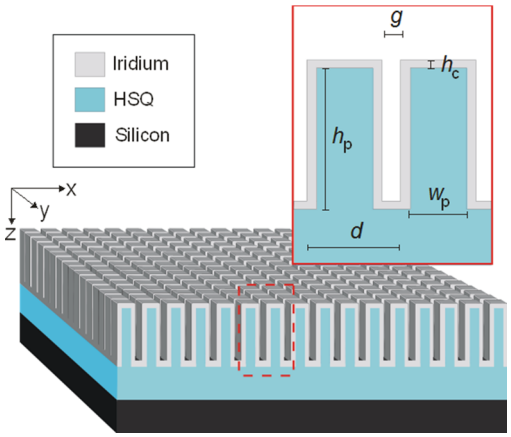

[a]The structure consists of high aspect ratio, iridium-coated dielectric (hydrogen silsesquioxane, HSQ) nanopillars with structural parameters defined as d = period, w_p= pillar width, h_p = pillar height, h_c = coating thickness, and g = interpillar gap width.

As we have investigated earlier, the confinement within the gap region can be achieved simply by tuning the period of the structure.[22] To demonstrate that this applies also for the iridium coated dielectric pillar structures, we simulated the situation using Fourier modal method (FMM)[23] with different periods, while keeping the other parameters (h_p= 500 nm, h_c = 20 nm) fixed. The results of the simulations, illustrating the local electric field enhancement around the pillar structures are shown in Figure 1. The field enhancement is calculated by dividing the time averaged energy density of the electric field with the energy density of the incoming field. The structures are illuminated by a plane wave under normal incidence (θ_i = 0°) at λ = 514 nm (the excitation wavelength of the SERS setup). As it can be seen in Figure 1a, most of the energy is concentrated on the top of the pillars, when d = 500 nm, whereas when d is reduced to 400 and 200 nm (Figures 1b and c), light becomes more confined within the interpillar gaps.

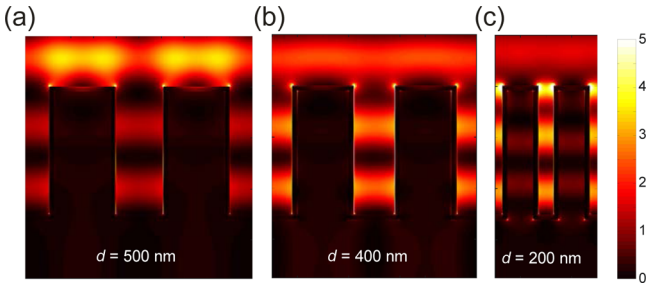

Figure 1. Simulated field enhancement, showing the distribution of the electric field for different structure periods. (a) d = 500 nm, (b) d = 400 nm, and (c) d = 200 nm. The simulations demonstrate how the confinement between the pillars is increased, when d is decreased.

This phenomenon can be explained by the coupling behavior of the incident light to different modes within the structure. When light impinges on the metal-coated nanopillars, both standing waves (cavity modes) and propagating SPPs (SPP modes) can be excited. However, when θ_i = 0°, the excitation of SPPs occurs only when the wave vectors of the grating and the SPP wave match. In other words, the excitation takes place when the period of the grating matches the wavelength of the surface plasmon polariton wave (λ_{SPP}) at the air-iridium interface. Because here λ_{SPP} = 507 nm, the excitation of SPPs dominates when the period is close to this wavelength, that is, d = 500 nm (see the Methods section for the calculation of λ_{SPP}). Thus, at this particular period, the SPP excitation prevents the effective coupling of the incident light to the cavity modes, resulting in only a small fraction of the energy to be stored within the interpillar gaps. However, when d deviates enough from λ_{SPP}, the effectively excited cavity modes, shaped in the form of standing waves, quickly predominate over the SPP modes. This predominance can be easily distinguished in Figure 1c, where the amplitude of the SPP wave at the air−iridium interface on top of the pillars is obviously weaker than that of the standing wave localized in gaps.

Now, to further increase the field enhancement within the gap region, the gap width is decreased by increasing the thickness of the iridium coating, while keeping d fixed at 200 nm (Figure 2). When h_c is increased and g is simultaneously decreased, the field gradually weakens at the bottom of the gaps and becomes more and more concentrated at the upper portion of the gap region (Figure 2a). A close-up on the upper part of the cavity (Figure 2b) shows how, at a large gap width (g = 60 nm), the field amplitude is high only at the immediate vicinity of the iridium surface, whereas with a small gap width (g = 5 nm), the intense field extends over the whole gap region because of near field coupling between the two closely spaced

DOI: 10.1021/acsami.5b02206
ACS Appl. Mater. Interfaces 2015, 7, 11452−11459

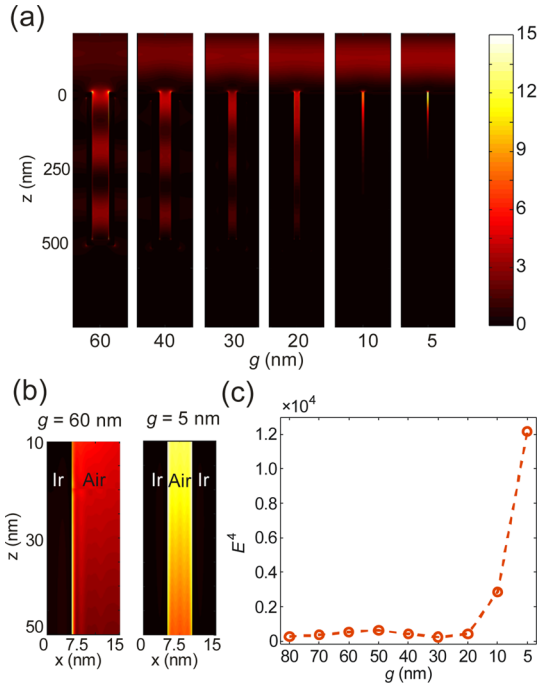

Figure 2. Simulated distribution of the electric field, when the thickness of the iridium coating is increased and the gap width (g) is simultaneously decreased. (a) The distribution with different values of g, (b) a close-up from the cavity, showing the field distribution at the immediate vicinity of the iridium surface with g = 60 and g = 5 nm.(c) The field enhancement to the power of four (E^4) with a decreasing gap width, estimating how the field enhancement correlates with the SERS enhancement.

pillars. In general, the field amplitude increase is quite moderate. However, keeping in mind that the SERS enhancement is in fact proportional to the fourth power of the field enhancement,[24] we estimated the expected SERS enhancement, as a function of gap width, by calculating the average field enhancement within the cavity raised to the power of four (E^4). As seen in Figure 2c, E^4 is quite small when g > 20 nm, but when g < 10 nm, E^4 starts to rise sharply. This indicates that also a moderate increase in the field enhancement can lead to a significant increase in the predicted signal enhancement when g is small enough.

Realization and Characterization of the Iridium-Coated Nanopillar Structures. On the basis of the theoretical simulations, a set of high aspect ratio iridium-coated pillar arrays with a fixed period, pillar width and height (d = 200 nm, w_p = 100 nm, and h_p = 500 nm) but a decreasing gap width g were fabricated by applying electron beam lithography (EBL) and ALD coating techniques. The former was employed to pattern dielectric skeleton pillars into a resist (hydrogen silsesquioxane, HSQ) and the latter to coat the pillars conformally with iridium films.[21] This kind of an approach was used because fabricating such subwavelength, high aspect ratio structures directly from iridium is extremely difficult. Furthermore, this approach conveniently results in structures with a slightly positively sloped profile, which is essential for the conformal growth in the subsequent ALD process, as it allows the precursor gases to reach the reaction surface more easily. The conformal growth itself is vital for achieving the <10 nm gap widths required for the optimal SERS performance.

In total, eight pillar samples and eight planar reference samples were coated with iridium. The thickness of the films was controlled by varying the number of ALD deposition cycles. The resulting film thicknesses and the corresponding interpillar gap widths are listed in Table 1.The fabricated

Table 1. Number of ALD Cycles versus the Measured Thickness of the Iridium Films (h_c) and the Resulting Nominal Gap Width (g)[a]

cycles	h_c (nm)	g (nm)
250	10.6	78.8
370	15.5	69.0
500	20.1	59.8
625	23.9	52.2
750	29.1	41.8
875	32.2	35.6
1050	41.2	17.6
1125	41.7	16.6

[a]See the Methods section for details on the film thickness measurement procedure.

structures and the quality of the iridium film were investigated by Scanning electron microscope (SEM) imaging. SEM micrographs of the fabricated nanopillars show that the pillars are slightly sloped and are more rounded at the top in comparison to the ideal structures investigated in the theoretical simulations (Figure 3). Furthermore, SEM images before and after the iridium ALD coating demonstrate how the film indeed grows conformally when employing ALD. However, even though the growth is conformal, a close up on two adjacent pillars shows that the film growth is not ideal but some nanoscale roughness can also be observed because the films are polycrystalline. Thus, although the gap between the coated structures is nominally 16.6 nm, it is clearly locally less than 10 nm because of the roughness of the film.

The roughness of the films was further investigated by using atomic force microscopy (AFM) imaging. For convenience, the AFM imaging was performed only on the planar reference films. It can be seen in Figure 3d that the thinnest film (10.5 nm) does not seem to fully cover the substrate and actually resembles a film of particles rather than a continuous film. The film clearly has voids between the grains/particles whereas with the thickest film (Figure 3e), the whole surface is completely covered by iridium. This behavior is typical for very thin metallic films, which tend to grow in an island-like fashion rather than the layer-by-layer mode, and this may be further emphasized by the rather inert nature of the HSQ surface. As a consequence, the roughness of the film decreases when the film is thick enough. For the thinnest film (10.5 nm), the surface roughness R_a = 4.4 nm was measured, whereas for the thickest film (42.7 nm) the roughness had reduced down to R_a = 1.4 nm.

All samples were also characterized by using a spectrophotometer to determine the optical (and plasmonic) properties of the structures. However, the obtained data did not show any dramatic changes in the reflectance spectra and the data was thus excluded. This was probably due to the fact that the structures are quite small (1 × 1 mm^2) and therefore difficult to measure accurately with a standard spectrophotometer.

SERS Experiments. The SERS enhancement properties of the iridium-coated nanopillar structures were evaluated by using rhodamine 6G (Rh6G), as it is the most commonly used model analyte in SERS research. After treatment of the samples with 1.0 μM Rh6G, Raman spectra were measured at 8 different

DOI: 10.1021/acsami.5b02206
ACS Appl. Mater. Interfaces 2015, 7, 11452−11459

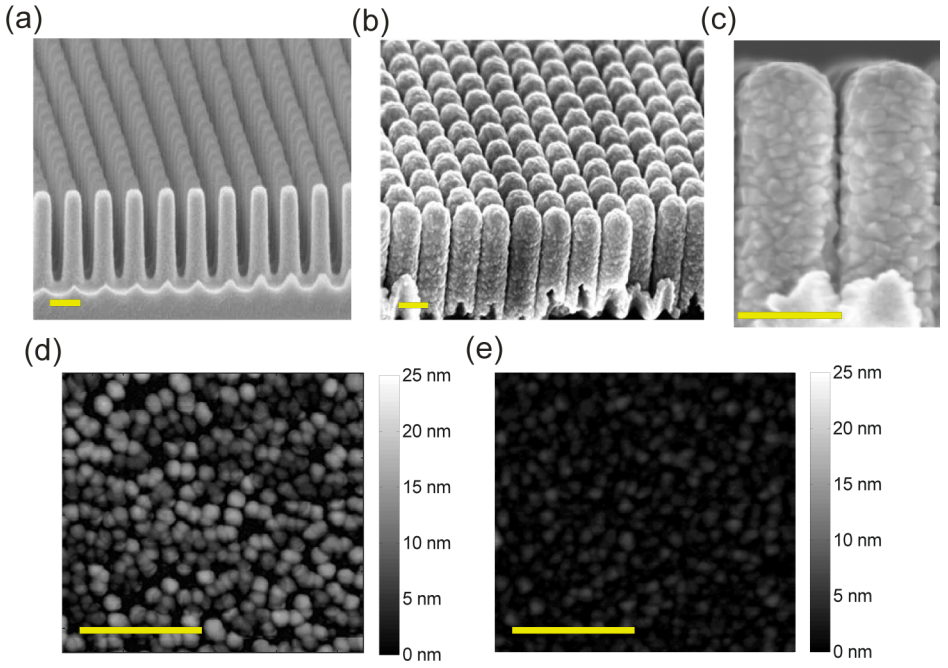

Figure 3. SEM micrographs of fabricated nanopillars (a) before and (b) after the iridium ALD coating and (c) a close-up of two adjacent pillars (42.7 nm thick iridium coating). The period and height of the pillars are d = 200 nm and h_p = 500 nm and the scale bar in all panels corresponds to 200 nm. AFM scans of the (d) 10.5 and (e) 42.7 nm thick iridium films showing how the morphology of films changes and the roughness decreases, when the film thickness is increased.

locations for each sample. In all the measurements, the excitation wavelength of 514 nm with an optical power of 50 μW, an exposure time of 10 s and a spot size of 5 μm were used(as a control 785 nm excitation was also tested but no signal from Rh6G could then be detected). In addition to nanopillar structures, we also studied SERS enhancement properties of the planar reference iridium films of the same thicknesses and pillar structures without iridium coating. However, no Raman peaks were observed with the uncoated reference pillars (data not shown).

The results of the SERS experiments for the iridium coated samples are shown in Figure 4.When the film is very thin (Figure 4a), both the planar reference (black curve) and the nanopillars (red curve) show Raman peaks of Rh6G at 1310, 1363, 1509, 1572, and 1650 cm^{-1}. However, as the film thickness is increased, the enhancement decreases until Raman peaks can no longer be distinguished from the reference (Figure 4b). However, the peaks reappear with the nanopillar samples, when the film is thick enough or in other words, the gap between the two adjacent pillars becomes very narrow (Figure 4c).

The high enhancement observed with the narrowest gaps (g = 17.6 and 16.6 nm) is consistent with the simulations (Figure 2), as the reducing gap width should result in a higher confinement, a higher energy density and thus higher signal enhancement. However, the sharp rise in the SERS signal intensity is observed "earlier" than expected. This is likely caused by the slightly sloped profile of the fabricated pillars (Figure 3), which results in slightly different gap widths at the bottom and the top of the cavities. Furthermore, in contrast to the SERS enhancement behavior predicted by the simulations, moderately strong SERS signals were observed also with the largest gaps (thinnest films). As the same behavior was observed both with the planar reference and the nanopillars, we assume that it is not caused by the pillar structures but by the film itself. We believe that the explanation lies in the morphology of the films: the thinnest films are more particle-like and are hence also rougher than the thicker ones (Figure 3). Thus, we assume that the enhancement is generated by the hot spots formed in the voids between the grains/particles of the relatively rough thin films. A similar observation was made earlier with silver films deposited by plasma enhanced ALD on planar substrates that exhibited plasmonic properties which depended strongly on the nanostructure of the Ag film.[25] Simulations indicated that this plasmonic behavior was due to air gaps left between silver grains in the mosaic-like microstructure of the PEALD Ag film. A similar explanation may be proposed for the present iridium films too, and the vanished Raman peaks in thicker iridium films therefore indicate closing of the gaps by grain coalescence when the film grows thicker and thus starts to behave more like an ideal metal film.

As a standard procedure, the signal enhancement properties of different SERS substrates are often compared by calculating their respective SERS enhancement factors.[26] Here, however, the calculation was impossible as the overwhelming fluorescence background of Rh6G obscured the peaks in normal Raman measurements. Thus, to put the obtained signal enhancement in a more general context, we compared the enhancement properties of our iridium based SERS substrates against two of our recently reported silver based SERS substrates. The silver substrates exploit silver coated polymer nanowrinkles[27] and uniformly distributed silver particles[16] for the signal enhancement generation. To make the comparison fair, all measurement were performed with exactly the same measurement parameters and the same rhodamine treatment (excitation wavelength = 514 nm, power = 50 μW, exposure time = 10 s and incubation in 1.0 μM Rh6G). It should be noted that Rh6G is close to resonance at 514 nm so additional enhancement is generated due to surface-enhanced resonance

DOI: 10.1021/acsami.5b02206
ACS Appl. Mater. Interfaces 2015, 7, 11452−11459

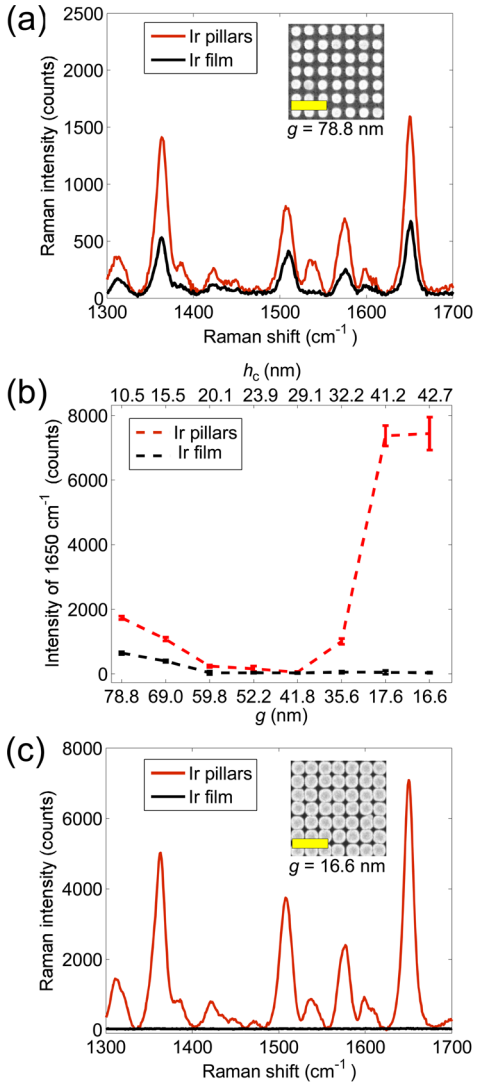

Figure 4. Baseline corrected Raman spectra of Rh6G measured on iridium pillar structures and on a reference, a planar iridium film, with different film thicknesses. (a) The spectra measured on a sample coated with 10.5 nm thick film of iridium. (b) Raman intensity as a function of film thickness (h_c) and the gap width (g), and (c) Raman spectra measured on samples coated with a 41.7 nm thick film of iridium. The insets in panels a and c are SEM images from the pillar structures with g = 78.8 and 16.6 nm, respectively. The scale bar in both images corresponds to 500 nm.

Raman scattering (SERRS).[28] However, as all samples are measured with the same excitation wavelength, the comparison is still valid.

The displayed spectra (Figure 5) for the iridium film and iridium nanopillars correspond to the ones that performed the best, that is, the thinnest film (10.5 nm) and the second narrowest gap (g = 17.6 nm), respectively. It can be seen the iridium film performs clearly worse than any of the other substrates. On the other hand, both of the silver substrates give higher enhancement than the iridium pillars. However, the difference is not very significant in terms of the magnitude of the signal enhancement.

However, in terms of the measurement repeatability there is a huge difference. The measurement-to-measurement signal intensity variation was only ±4% with the best iridium nanopillar substrate, which means that the measurement repeatability was three times better than with the silver nanowrinkles and five times better than with the silver particle based substrate. Although similar degree of repeatability has already been reported at least with some silver based structures,[29] this low variation is in general very rarely achieved. Here, the repeatability is actually pushing the limit of the measurement system itself, for which we measured on an average ±5% signal intensity variation using a silicon reference and exactly the same measurement parameters as in the SERS experiment (see the Methods and Supporting Information Figure S1 for details). Furthermore, this degree of repeatability was not only observed with this particular sample but could be seen with all samples, which generated detectable Raman signal from the Rh6G molecules. On average, the measurement-to-measurement repeatability was ±6% for five different samples (Supporting Information Table S1). The repeatability originates from the uniform distribution of hot spots within interpillar gaps, which is made possible by using the state-of-the-art fabrication processes. We also can assume that the reproducibility of the fabrication process itself is excellent, as the two, nearly identical samples with 17.6 and 16.6 nm nominal gap widths (Figure 4b) produced practically identical enhancements.

Of course, it should be noted that the morphologies of the iridium and silver substrates differ significantly and the reference SERS substrates investigated here may not represent the most optimally performing of all silver-based SERS substrates. However, by measuring the enhancement properties with the same measurement device (using the same measurement parameters and sample preparation procedures) for all SERS substrate candidates, we could compare how well each substrate performed under these conditions. Thus, we are not claiming that iridium is superior to silver as a metal/material for SERS but that if the structures are designed and fabricated properly, they can perform just as well in terms of signal enhancement.

The use of iridium has also some general advantages. First of all, it is corrosion resistant like gold and therefore its enhancement properties do not degenerate on their own like those of silver. In addition, iridium (unlike gold at the moment due to the lack of suitable precursor materials[30]) can be grown using ALD, which enables both conformal and highly accurate metal deposition and as a consequence, the dimensions of the hot spots can be controlled very precisely. This kind of corrosion resistant, highly reliable SERS structures could be beneficial in different hazardous environments, where durable and accurate sensors are required.

Of course the fabrication cost of this kind of SERS substrate can be quite high, as both EBL and ALD require expensive instrumentation. However, if the patterning generated by EBL is transferred to polymers by roll-to-roll imprinting[31] for example, large quantities of pillar structures can be fabricated by using a single EBL patterned master. In addition, also ALD is mass production compatible: even standard ALD machines can be applied to coat large quantities of patterned structures simultaneously and the most modern ALD equipment are actually capable of roll-to-roll coating.[32] Thus, when combined with modern mass fabrication methods, the fabrication cost of the iridium SERS structures could be brought down to a very feasible level.

DOI: 10.1021/acsami.5b02206
ACS Appl. Mater. Interfaces 2015, 7, 11452−11459

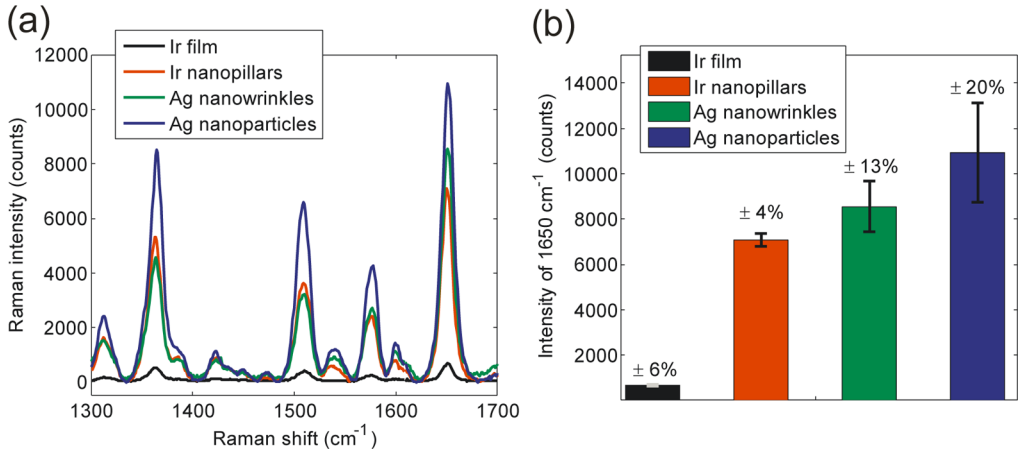

Figure 5. Comparison of the SERS performance of iridium and silver based SERS substrates using the same measurement parameters and the same Rh6G treatment. (a) Baseline corrected Raman spectra of Rh6G and (b) Raman signal intensities and variations (standard deviation, n = 8) at 1650 cm^{-1}.

METHODS

Theoretical Simulations. All numerical simulations in this study are based on Fourier Modal Method (FMM). The structures were illuminated with a plane wave directed along the z-axis with $\theta_i = 0°$, λ = 514 nm and polarization parallel with the x-axis (Scheme 1). Diffraction orders from −50 to 50 were taken into account in all simulations. The field enhancement was calculated by dividing the time averaged energy density (ω) of the electric field with the time averaged energy density of the incoming field (ω_0). The SERS enhancement was estimated by calculating the fourth power of the average field enhancement within the upper portion of the cavity (see Supporting Information Figure S2 for details).

The SPP wavelength λ_{SPP} was calculated using the equation

$$\lambda_{SPP} = \lambda \sqrt{\frac{n_m^2 + n_i^2}{n_m^2 \cdot n_i^2}} \quad (1)$$

where n_i is the refractive index of the incident medium (air), n_m is the refractive index of the metal (iridium), and λ is the excitation wavelength. In the calculation, we used values of n_i= 1 and n_m = 2.10 + 4.05i[33]and λ = 514 nm.

Fabrication of the Iridium Pillar Structures. In fabrication of the dielectric pillars, a simple etching free processing was applied in order to ensure a high aspect ratio of the structures with a slightly positively sloped profile. Resembling properties with silicon dioxide were exploited by fabricating the pillars using a hydrogen silsesquioxane (HSQ) spin-on dielectric (FOX-16 from Dow Corning), which acted as a negative tone resist that can be patterned using electron beam radiation. The patterning was performed on spin-coated HSQ with a thickness of approximately 590 nm on a silicon wafer using electron beam patterning tool Vistec EBPG 5000+ES HR. Exposure was made with an acceleration voltage of 100 kV enabling small forward scattering and thus favoring the sidewall profile in target. The applied exposure dose was set to 9000 $\mu C/cm^2$ and the patterned resist was developed using NaOH based chemistry using MP 351 developer diluted in water in ratio of 1:3. To avoid falling of the pillars, the resist was not developed completely through. Thus, an undeveloped residual layer was left behind as a stabilizing footing at the base of the pillars.

Iridium was grown on the high aspect-ratio dielectric pillars by ALD at 300 °C from $Ir(acac)_3$ (acac = 2,4-pentanedione) and O_2 (99.999%) for 250−1220 cycles.[21] Films were grown in a F120 reactor (ASM Microchemistry, Ltd., Finland) and nitrogen was used as a carrier and a purging gas. The number of ALD cycles, corresponding to the different thicknesses is listed in Table1.

Sample Characterization. The thickness of the iridium films was studied with a Hitachi S-4800 field emission scanning electron microscope and an INCA 350 EDX spectrometer. The film thicknesses were determined from the reference Si(100) samples and were calculated using a GMR electron-probe thin film microanalysis program with bulk densities for Ir. SEM imaging of the pillar structures was performed using SEM LEO 1550 Gemini scanning electron microscope with an acceleration voltage of 5 kV. AFM imaging and roughness analysis were done using Multimode 8 atomic force microscope from Bruker.

Raman Measurements and Data Processing. The SERS measurements were performed using Renishaw InVia Raman microscope and rhodamine 6G (Rh6G) as the target molecule. Prior to measurements, 20 μL droplet of Rh6G (1.0 μM) was deposited on all samples and after 20 min, the excess Rh6G was removed using an air blow. Thus, only the Rh6G molecules that had passively adsorbed on the surface during the 20 min contributed to the measured signal. Furthermore, when Rh6G is deposited in this manner, the refractive index within the gap region does not change remarkably and therefore the results of the simulations should hold also in the presence of analyte molecules. For each sample, Raman spectra were recorded from eight locations at the excitation wavelength of 514 nm, optical power of 50 μW, exposure time of 10 s and spot size of 5 μm using a 20×, NA = 0.40 objective. Finally, the spectra were baseline corrected and then averaged. The silver reference substrates were fabricated in-house. The measurement repeatability of the InVia Raman microscope was evaluated by measuring Raman-signal from a reference Si (100) sample using the same measurement parameters as in the SERS experiments.

CONCLUSION

In summary, we proposed a new type of SERS substrate that is based on symmetrically organized iridium coated nanopillars. The goal of this kind of a symmetric grating structure was to provide a uniform distribution of signal enhancing hot spots over a large surface area so that the signal enhancement could be as repeatable as possible. On the basis of rigorous simulations, the pillar structures were designed to support cavity modes between the pillars, that is, confine light and its energy within the interpillar gaps. However, according to the simulations, this local field enhancement was significant only if the width of the gap was very narrow (<10 nm). Thus, in order to create such conformal coatings and small gap widths, the structures were fabricated using iridium atomic layer deposition. We demonstrated through experimental measurements that the measured SERS enhancement indeed correlates well with the field enhancement predicted by the simulations, as the Raman signal intensity was strong only when the gaps were

DOI: 10.1021/acsami.5b02206
ACS Appl. Mater. Interfaces 2015, 7, 11452−11459

very narrow. Finally, to put the enhancement in more general context, we compared the signal enhancement generated by the iridium pillars against silver based SERS substrates. Remarkably, the enhancement achieved with the iridium based substrates was actually quite comparable to the enhancement observed on reference, silver substrates. Most notably, however, measurement-to-measurement repeatability was superior (±4%) with the iridium pillars in comparison to all reference substrates. Thus, we strongly believe that the reported fabrication approach can make quantitative SERS measurements easier to achieve. Furthermore, because of the ease of deposition and its inherent corrosion resistance, iridium itself can be a promising alternative as a base material for different kinds of plasmonic sensors.

■ ASSOCIATED CONTENT

Supporting Information

Repeatability of the measurement system evaluated using a polished silicon reference sample and the estimation of the SERS enhancement behavior are demonstrated in Figure S1 and S2, respectively, and average Raman intensities at 1650 cm^{-1} and the corresponding signal intensity variations for the iridium samples with different gaps widths are listed in Supplementary Table 1.The Supporting Information is available free of charge on the ACS Publications website at DOI: 10.1021/acsami.5b02206.

■ AUTHOR INFORMATION

Corresponding Author

*E-mail: kgg@bit.edu.cn.

Notes

The authors declare no competing financial interest.

■ ACKNOWLEDGMENTS

We gratefully thank Dr. Khaled Kaja and Bruker for the AFM measurements. Work at Beijing Institute of Technology was funded by the National Science Foundation of China (Grant No. 61205053). Work at University of Eastern Finland and at University of Helsinki was supported by the Finnish Funding Agency for Technology and Innovation (TEKES) and the Academy of Finland (grants 272155, 250968, 251142, and 284909). The research was also supported by the Finnish Center of Excellence in Atomic Layer Deposition.

■ REFERENCES

(1) Jun, Y. C.; Huang, K. C.; Brongersma, M. L. Plasmonic Beaming and Active Control over Fluorescent Emission. *Nat. Commun.* **2011**, *2*, 283.

(2) Kauranen, M.; Zayats, A. V. Nonlinear Plasmonics. *Nat. Photonics* **2012**, *6*, 737−748.

(3) Kim, S.; Jin, J.; Kim, Y. J.; Park, I. Y.; Kim, Y.; Kim, S. W. High-Harmonic Generation by Resonant Plasmon Field Enhancement. *Nature* **2008**, *453*, 757−760.

(4) Barnes, W. L.; Dereux, A.; Ebbesen, T. W. Surface Plasmon Subwavelength Optics. *Nature* **2003**, *424*, 824−830.

(5) Mcmahon, J. M.; Henzie, J.; Odom, T. W.; Schatz, G. C.; Gray, S. K. Tailoring the Sensing Capabilities of Nanohole Arrays in Gold Films with Rayleigh Anomaly-Surface Plasmon Polaritons. *Opt. Express* **2007**, *15*, 18119−18129.

(6) Bukasov, R.; Ali, T. A.; Nordlander, P.; Shumaker-Parry, J. S. Probing the Plasmonic Near-Field of Gold Nanocrescent Antennas. *ACS Nano* **2010**, *4*, 6639−6650.

(7) Svedendahl, M.; Chen, S.; Dmitriev, A.; Kall, M. Refractometric Sensing Using Propagating Versus Localized Surface Plasmons. *Nano Lett.* **2009**, *9*, 4428−4433.

(8) Jain, P. K.; El-Sayed, M. A. Noble Metal Nanoparticle Pairs: Effect of Medium for Enhanced Nanosensing. *Nano Lett.* **2008**, *8*, 4347−4352.

(9) Kim, H. M.; Jin, S. M.; Lee, S. K.; Kim, M. G.; Shin, Y. B. Detection of Biomolecular Binding through Enhancement of Localized Surface Plasmon Resonance (LSPR) by Gold Nanoparticles. *Sensors* **2009**, *9*, 2334−2344.

(10) Tripathy, S.; Mlayah, A. Dual Wavelength Sensing Based on Interacting Gold Nanodisk Trimers. *Nanotechnology* **2010**, *21*, No. 305501.

(11) Nie, S. M.; Emory, S. R. Probing Single Molecules and Single Nanoparticles by Surface-Enhanced Raman Scattering. *Science* **1997**, *275*, 1102−1106.

(12) Kneipp, J.; Kneipp, H.; Kneipp, K. SERS—A Single-Molecule and Nanoscale Tool for Bioanalytics. *Chem. Soc. Rev.* **2008**, *37*, 1052−1060.

(13) Talley, C. E.; Jackson, J. B.; Oubre, C.; Grady, N. K.; Hollars, C. W.; Lane, S. M.; Huser, T. R.; Nordlander, P.; Halas, N. J. Surface-Enhanced Raman Scattering from Individual Au Nanoparticles and Nanoparticle Dimer Substrates. *Nano Lett.* **2005**, *5*, 1569−1574.

(14) Prokes, S. M.; Glembocki, O. J.; Rendell, R. W.; Ancona, M. G. Enhanced Plasmon Coupling in Crossed Dielectric/Metal Nanowire Composite Geometries and Applications to Surface-Enhanced Raman Spectroscopy. *Appl. Phys. Lett.* **2007**, *90*, No. 093105.

(15) Xu, H.; Bjerneld, E. J.; Kall, M.; Borjesson, L. Spectroscopy of Single Hemoglobin Molecules by Surface Enhanced Raman Scattering. *Phys. Rev. Lett.* **1999**, *83*, 4357−4360.

(16) Matikainen, A.; Nuutinen, T.; Vahimaa, P.; Honkanen, S. A Solution to the Fabrication and Tarnishing Problems of Surface-Enhanced Raman Spectroscopy (SERS) Fiber Probes. *Sci. Rep.* **2015**, *5*, No. 8320, DOI: 10.1038/srep08320.

(17) Ren, B.; Lin, X.; Yang, Z.; Liu, G.; Aroca, R. F.; Mao, B.; Tian, Z. Surface-Enhanced Raman Scattering in the Ultraviolet Spectral Region: UV-SERS on Rhodium and Ruthenium Electrodes. *J. Am. Chem. Soc.* **2003**, *125*, 9598.

(18) Abdelsalam, M. E.; Mahajan, S.; Bartlett, P. N.; Baumberg, J. J.; Russell, A. E. SERS at Structured Palladium and Platinum Surfaces. *J. Am. Chem. Soc.* **2007**, *129*, 7399.

(19) Chakrapani, K.; Sampath, S. Spontaneous Assembly of Iridium Nanochain-like Structures: Surface Enhanced Raman Scattering Activity Using Visible Light. *Chem. Commun.* **2014**, *50*, 3061−3063.

(20) Leskelä, M.; Ritala, M. Atomic Layer Deposition (ALD): From Precursors to Thin Film Structures. *Thin Solid Films* **2002**, *409*, 138−146.

(21) Aaltonen, T.; Ritala, M.; Sammelselg, V.; Leskela, M. Atomic Layer Deposition of Iridium Thin Films. *J. Electrochem. Soc.* **2004**, *151*, G489−G492.

(22) Kang, G.; Dong, J.; Vartiainen, I.; Paakkonen, P.; Turunen, J. Investigation of Inverse Polarization Transmission through Subwavelength Metallic Gratings in Deep Ultraviolet Band. *Opt. Commun.* **2013**, *311*, 33−37.

(23) Kim, H.; Park, J.; Lee, B. *Fourier Modal Method and Its Applications in Computational Nanophotonics*; Tailor & Francis Group: Boca Raton, FL, 2012.

(24) Moskovits, M. *Surface-Enhanced Raman Spectroscopy: A Brief Perspective*; Springer: Berlin, 2006.

(25) Prokes, S. M.; Glembocki, O. J.; Cleveland, E.; Caldwell, J. D.; Foos, E.; Niinisto, J.; Ritala, M. Spoof-like Plasmonic Behavior of Plasma Enhanced Atomic Layer Deposition Grown Ag Thin Films. *Appl. Phys. Lett.* **2012**, *100*, No. 053106.

(26) Le Ru, E. C.; Blackie, E.; Meyer, M.; Etchegoin, P. G. Surface Enhanced Raman Scattering Enhancement Factors: A Comprehensive Study. *J. Phys. Chem. C* **2007**, *111*, 13794−13803.

(27) Stenberg, H.; Matikainen, A.; Daniel, S.; Nuutinen, T.; Stenberg, P.; Honkanen, S.; Pakkanen, T.; Vahimaa, P.; Suvanto, M. Self-Organized Polymer Wrinkles: A Lithography-Free Pathway for

DOI: 10.1021/acsami.5b02206
ACS Appl. Mater. Interfaces 2015, 7, 11452−11459

Surface-Enhanced Raman Scattering (SERS) Substrates. *Macromol. Mater. Eng.* **2015**, DOI: 10.1002/mame.201400391.
(28) Le Ru, E. C.; Etchegoin, P. G. *Principles of Surface Enhanced Raman Spectroscopy (and Related Plasmonic Effects)*; Elsevier: Amsterdam, 2009.
(29) Cho, W. J.; Kim, Y.; Kim, J. K. Ultrahigh-Density Array of Silver Nanoclusters for SERS Substrate with High Sensitivity and Excellent Reproducibility. *ACS Nano* **2012**, *6*, 249.
(30) Hamalainen, J.; Ritala, M.; Leskela, M. Atomic Layer Deposition of Noble Metals and Their Oxides. *Chem. Mater.* **2014**, *26*, 786−801.
(31) Ahn, S. H.; Guo, J. L. High-Speed Roll-to-Roll Nanoimprint Lithography on Flexible Plastic Substrates. *Adv. Mater.* **2008**, *20*, 2044−2049.
(32) Ali, K.; Choi, K. Low-Temperature Roll-to-Roll Atmospheric Atomic Layer Deposition of Al_2O_3 Thin Films. *Langmuir* **2014**, *30*, 14195.
(33) Lehmuskero, A.; Kuittinen, M.; Vahimaa, P. Refractive Index and Extinction Coefficient Dependence of Thin Al and Ir Films on Deposition Technique and Thickness. *Opt. Express* **2007**, *15*, 10744−10752.

DOI: 10.1021/acsami.5b02206
ACS Appl. Mater. Interfaces 2015, 7, 11452−11459